Validation of Negative Ion Beam Space Charge Compensation

Marco Cavenago*[1] and Pierluigi Veltri[2]
[1]INFN/LNL, Lab. Nazionali di Legnaro, [2]Consorzio RFX, Assoc. Euratom-ENEA
*Corresponding author: v. Universitá 2, I-35020 Legnaro (PD) Italy, cavenago@lnl.infn.it

Abstract: The transport of intense ion beams with reduced beam divergence over reasonable drift distances requires a reliable space charge compensation (SCC). Negative ion beams (required in the Neutral Beam Injectors envisioned for the ITER tokamak) are here discussed. Secondary particles are generated by beam-gas collisions within the beam volume and their motion is followed by explicit leapfrog time integration until they reach boundaries; when many beamlets are simulated, a fraction of the particle exiting the lateral boundaries is injected again. Poisson equation is solved and fields are accurately retrieved by Comsol Multiphysics at each time integration step; accurate choice of simulation parameters and speeding up techniques are used. Results show the formation of a SCC channel where the beam passes, after a short transition region at drift begin. The channel sides show double charge layers. These results fully confirm results of a preliminary fluid model, and cross validation of both codes is discussed.

Keywords: ion beams, secondary beam

1 Introduction

The Space Charge Compensation (SCC) is considered to be a key ingredient of the transport of high current ion beams in drift regions (regions with no acceleration field) [1, 2, 3, 4]. The phenomenon consists in the accumulation of a background charge that completely balances the beam space charge, allowing transport of nearly parallel beams without external focusing or acceleration. The transition between the acceleration and the drift region is a critical one, since the background charge may flow into the accelerator; this paper presents detailed simulations, which confirm the results of a previous previous fluid model[5] and allow to map the transition region and the beam propagation channel.

A large ion beam application is the IFMIF project, where a 125 mA beam of H^+ is transported between the ion source preacceleration (PA) and the 2m away accelerator[2] by the SCC with help of two solenoids. Another example is the Neutral Beam Injector where a matrix of 1280 beamlets (each consisting in 40 mA of D^-, or in preliminary tests H^-) is transported by SCC for 1.5 m from the electrostatic accelerator to a beam converter, the so-called neutralizer[6, 7, 8, 9].

A scheme of the typical geometry is shown in Fig. 1. In this principle studies, we consider a 2D (two dimensional) zx geometry and we choose simulation domains as simpler as possible (a rectangle or two rectangles). Future application may suggest the use of tapered electrodes.

For negative ions, we can consider only two major collision process, called background gas ionization and primary beam stripping

$$\underline{H}^{\pm} + H_2 \rightarrow \underline{H}^{\pm} + e + H_2^+ \qquad (1)$$

$$\underline{H}^{-} + H_2 \rightarrow \underline{H}^{0} + \underline{e} + H_2 \qquad (2)$$

where we mark with an underline the fast particles that approximately maintain the incoming H^- velocity v_b. We may have the sum of these two processes in one collision. The effective collision cross sections are about $\sigma_1 = 2\times10^{-20}$ m^{-2} and $\sigma_2 = 3\times10^{-20}$ m^{-2} for 100 keV H^- [10, 11]. Particles produced in the reaction are usually called secondaries, as opposite to the primary particles, here $H^{\pm}$.

Since for eq. 2 the electron typically maintains the incoming H^- velocity and rapidly exits from the simulation domain, eq. 2 has no net effect on the SCC. On the other side, in eq. 1 the electron gets only an energy up to 10 eV and H_2^+ speed is not much

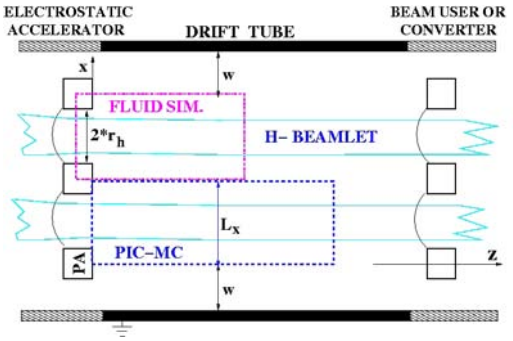

Figure 1: A scheme (not to scale) of the regions near the drift tube, comparing the simulation domains of fluid and PIC-MC models

greater than the gas one[4] (both with randomly directed velocities). As a result, electrons leave rapidly the simulation domain while H_2^+ stay longer. This accumulation of positive charge clearly shields the negative beam, and it may continues until total electric potential ϕ is positive enough (respect to drift tube walls) to trap some electrons; that is to say, the beam is overcompensated.

For positive ion beams, the positive self potential pushes H_2^+ away and traps some electrons, which are the background charge in this case; equilibrium may be reached when the total potential ϕ is slightly positive and the beam space charge is slightly under compensated.

From 1D model of radial transport, where $\phi_{,z} =$ is assumed, it is known that SCC appears over a critical gas pressure that should be anyway minimized for economy of gas pumping and to reduce beam collisions. The simulation of 2D or 3D devices necessary for a realistic beam transport is much more challenging. Our fluid model[5] shows a transition length of a few cm, and a clear double charge layer at the beam edge.

This fluid model was implemented in a Comsol Multiphysics (CM) environment, using several General PDE application modes, namely: u the electric potential (scaled), n_2 the density of H_2^+ ions, v_x and v_z their fluid velocity; the capability of treating mixed boundary conditions was used to represent one or many beamlet systems. Here particles are generated by a Particle in Cell Monte Carlo approach (PIC-MC) [12], and moved by a leap-frog method, using Comsol Multiphysics routines to compute the electric potential ϕ on a dense mesh and the field at each particle location.

Detailed results for SCC should also help larger scope codes, like BYPO [13, 14], where source extraction, acceleration and drift region are modeled, in place of the simplified SCC model currently used.

In section II, the basic equations and boundary conditions are summarized; some details on programming efficiency, of noise variance reduction techniques and of primary beam profiles are also given. Section III show remarkable results of some simulations and compares them to fluid model results. Section IV discuss perspective of synergies between fluid and PIC-MC models.

2 Basic equations and assumptions

Let $n_2(z,x,t) = n_{H_2^+}$ be the density of H_2^+ ions (depending also on time t) and n_e the density of electrons. The code uses a 2D planar geometry; in the example here reported some parameters are set up to meet the SPIDER [9] accelerator features: the gas density is $n_g = 2 \times 10^{18}$ m^{-3} and the acceleration voltage is $U_b = 100$ kV.

We assume that primary ions are parallel to z axis, which is approximately verified for short enough simulation domains and for well designed accelerators. In detail, $v_z = v_b = 4.4 \times 10^6$ m/s and the primary beam density is $n_{H-} = n_0 n_b(x)$, where n_0 is its maximum density and n_b is an user assigned profile. In order to speed up preliminary simulations, a reduced $n_0 = 8.2 \times 10^{13}$ m^{-3} is used; let $2r_b = 8$ mm be the beam width. The attenuation length of the H^- beam is $1/(\sigma_2 N_g) = 16$ m; in the considered simulation domain $0 < z \leq L_z = 0.25$ m the beam attenuation is small (about 1.5 %), so we can assume a constant primary beam, allowing for a SCC axial equilibrium $\partial_z n_2 = 0$ at the right side (the beam exit).

The Poisson equation is

$$-(\epsilon_0/e) \triangle \phi = n_2 - n_e - n_0 n_b \equiv n_0 n_a \quad (3)$$

where n_a measures the local charge compensation (a 100 % compensation gives $n_a = 0$). We also define

$$Q_2(t) = \int n_2(z,x,t)\,\mathrm{d}x\,\mathrm{d}z/(2r_b n_0) \quad (4)$$

$$Q_e(t) = \int n_e(z,x,t)\,\mathrm{d}x\,\mathrm{d}z/(2r_b n_0) \quad (5)$$

which are global measures of the compensation progress.

The rate density of secondary production is

$$R_s = \mathrm{d}n_2 \,/\, \mathrm{d}t \, = n_g n_0 n_b(x) \sigma_1 \qquad (6)$$

So that an effective density of secondary $n_s = R_s \, \mathrm{d}t$ is created at each time step, and divided into an suitable number of macroparticles whose positions are chosen randomly inside the beam region with a velocity depending on particles species.

We assume that secondary electron velocity at production is distributed according to a Maxwellian with temperature (in energy units) $T_e \cong 3$ eV; similarly the ion temperature at start be T_i. Ion temperature origins include the gas temperature $T_g \cong 0.18$ eV. Reasonably larger T_i are usually assumed to improve code stability. An important scale is the Debye length $\lambda_D = (\epsilon_0 T_e / e^2 n_0)^{1/2}$; here $\lambda_D = 1.4$ mm for the low beam density used. To faithfully represent Poisson equation in the discretization, we need $h_x = h_z \leq l_D/2$ where h_x and h_z are the mesh sizes; conservatively we use a square grid with $h_x = 0.17$ mm. Since $r_b \gg \lambda_D$, from fluid model we can expected $n_a \cong 0$ at beam center, and n_a comparable with one half within distances λ_D from beam edge.

Let N_2 the number (bound by user choice, here to less than 2×10^5) of macroparticles representing H_2^+ and w_2 the number of ions which each macroparticle represents; clearly $q_2 = w_2 e$ and $m_2 = w_2 m_{H2}$; motion equations are

$$m_2 \, \mathrm{d}_t \mathbf{v} = q_2 \mathbf{E}(\mathbf{x}) \quad , \quad \mathrm{d}_t \mathbf{x} = \mathbf{v} \qquad (7)$$

for each ion macroparticle (with position $\mathbf{x}$ and velocity $\mathbf{v}$). A leap frog method is used, and is easily vectorized in the scripting language[15], calling Comsol Multiphysics routines for $\mathbf{E}$ calculation[15]. For simplicity the integration time step $\mathrm{d}t_1$ is (up to now) taken equal for electron and ions, according to $\mathrm{d}t_1 \leq \lambda_D / v_e^{th}$ with v_e^{th} the thermal electron velocity. Since there are spatial scales smaller than λ_D, namely the mesh size h_x and physically the beam edge thickness δ_b, $\mathrm{d}t_1 = 1.2$ ns is fairly large for electrons, which are anyway the minority. For ions, $\mathrm{d}t_1$ is safely small. Space charge and ϕ are updated each time step; space charge is smoothed (rectangular kernel) within a distance $w_s = 5 h_x = 0.85$ mm.

An estimate of the total number of H_2^+ is $A n_0 L_y$ where $A = 2 r_b L_z$ is the beam area and $L_y = 1$ m is a conventional extension in the ignored coordinate y; so that we set $w_2 = A n_0 L_y / N_2$; in our example $w_2 = 1.1 \times 10^6$. The scale of the interaction energy $\mathcal{E}_M = q_2^2 / 2\pi\epsilon_0 L_y$ between two macroparticles gives a first idea of the real ion energy resolution of our simulations $\delta T_i \gg \mathcal{E}_M / w_2$ which equals 0.0032 eV; observed noise is much larger, notwithstanding some smoothing.

2.1 Boundary conditions

At the lower ($x = 0$) and upper ($x = L_x$) boundaries, we have (exactly or approximately) as shown before[5]:

$$\mathbf{n} \cdot \nabla u = -i_w u \qquad (8)$$

where i_w is set according to the cases: 1) for the case of an infinite array of beamlets, we have symmetry at upper and lower boundaries, so $i_w = 0$; 2) for one beamlet only in drift tube , $i_w \cong 1/w$, where w is the distance between the domain boundary and the actual wall; typical values are $L_x = 22$ mm and a drift tube width 62 mm , giving $w = 20$ mm, which demonstrates a 65 % reduction in the simulation domain area and a considerable speed up; 3) for many beamlets in the same drift tube, i_w may depend on boundary.

At the exit plane $z = z_h$, (in the middle of an open space like the drift tube) a simple Neumann condition is appropriate. The input plane $z = 0$ cuts the PA electrode and the beam input hole. Of course at the PA we have a fixed potential $\phi = \phi_{PA}$, measured respect to the drift tube; typically $\phi_{PA} = 0$. On the beam hole, it is difficult to propose a simple boundary condition (for the several effects discussed in the fluid model[5], where a part of the PA hole was indeed included, see here Fig. 1). Anyway with large approximation we may consider that most of the primary beam charge will be compensated, resulting in weak fields; so that E_z is weakly bound to zero, but ϕ is free. Joining these regions, in Comsol Multiphysics we set a Dirichlet condition at $z = 0$, with $G = 0$ and

$$0 = R = (\phi_{PA} - \phi) \Theta(|x - \tfrac{1}{2} L_x| - r_h, w_h) \qquad (9)$$

where the smoothed Heaviside function Θ is given by the inbuilt function 'flc2hs', r_h

is the beam hole radius (7 mm here) and $w_h = 0.5$ mm is a smoothing distance. As a verification, note that inside beam hole, Θ is zero, so that ϕ is not constrained to ϕ_{PA}.

The boundary condition for particle flow at $z = z_h$ is free symmetric and specular flow; that is, when a particle exit with velocity (v_z, v_x) another one is injected with initial velocity $(-v_z, v_x)$; this is consistent with the Neumann condition for ϕ, since it maintains an uniform SCC at this boundary.

At the PA, particles are lost: physically our low energy electron enters in the metal and ions are neutralized, making two H atoms. In the beam hole, particle fate depends on the selfconsistent solution for ϕ; typically ion flows freely, reaching the accelerator region; that is, ions are lost; electron are reflected. This cases are easily implemented in the scripting language.

At the lower and upper boundary (of the simulation domain), a fraction F_c of particle may be reflected. In the many beamlet case $F_c > 0$ indicates recirculation of secondaries from one beamlet to another. In the single beamlet case, $F_c \cong 0$; its exact value depends selfconsistently on the ϕ value. For positive ϕ, H_2^+ ions which arrive at $x = L_x$ will continue to drift tube walls, so that $F_c = 0$ exactly. For electrons with small speed $F_c = 1 - \exp(-\phi(z, L_x)/T_e)$ since it is still possible that they attracted back to the beam, possibly returning to a different z. This latter case for F_c is to be rapidly implemented (also in the fluid model); we take $F_c = 0$ in the following.

2.2 Implementation

Code largely benefit from parallelization of Comsol Multiphysics routines, even if some careful programming is required for efficiency. In detail, the assembly phase is critical, since the user function 'dens(x,y)' representing the smoothed $(n_2 - n_e)/\epsilon_0$ is called many times by 'assemble'; this number was reduced by increasing 'blocksize'. It should be realized that computations contained in 'dens' are repeated over all the 2D region nodes, even if 'dens(x,y)' is called for a few points; the obvious and effective solution is to perform most computations before 'dens' is called. Other optimization modes, like reusing the same stiffness matrix on all Poisson solver calls, give additional, but comparatively smaller speed gains, at the price of more obscure programming; user may switch between these modes at any time.

The predefined beam profiles (in the order, flat, trapezoidal, gaussian and parabolic) are symmetric respect to the $x = \frac{1}{2}L_x$, so using the shorthand $x' = |x - \frac{1}{2}L_x|$, they are easily written as

$$\begin{aligned} n_{b1} &= \Theta(r_b - x') \\ n_{b2} &= \max(0, \min[1, \tfrac{1}{2} + (r_b - x')/\delta_b]) \\ n_{b3} &= \exp[-\tfrac{1}{2}(x'/\sigma_b)^2] \\ n_{b4} &= \max(0, 1 - (c_4 x'/r_b)^2) \end{aligned} \tag{10}$$

where δ_b is the thickness of the region where n_{b2} goes from 1 to 0.

To maintain the normalization $\int n_b(x)\,\mathrm{d}x = 2r_b$ we set $c_4 = \frac{2}{3}$ and $\sigma_b = r_b(2/\pi)^{1/2}$.

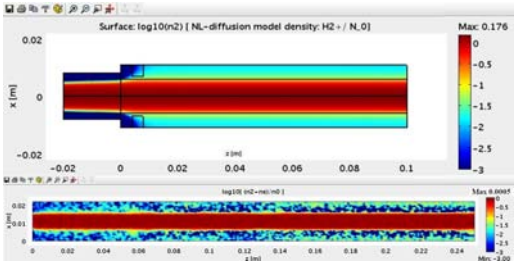

Figure 2: Upper panel: map of the normalized ion density, from fluid model. Lower panel: map of the normalized densities $(n_2 - n_e)/n_0$, from PIC-MC. To enhance graph visibility, we plot the decimal log, with a minimum displayed of 0.001

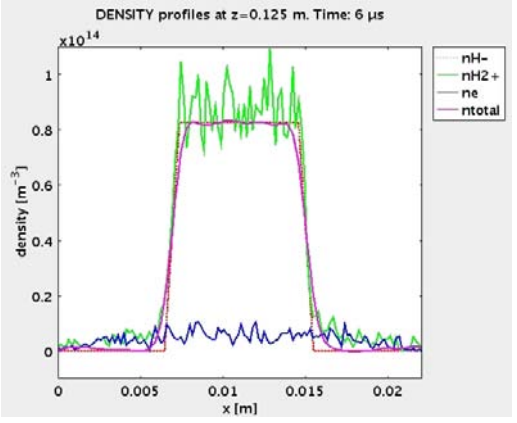

Figure 3: Profile of densities at the middle section $z = \frac{1}{2}z_h$; density of primary n_{H-} has a trapezoidal shape, 'ntotal' is $n_2 - n_e$, smoothed

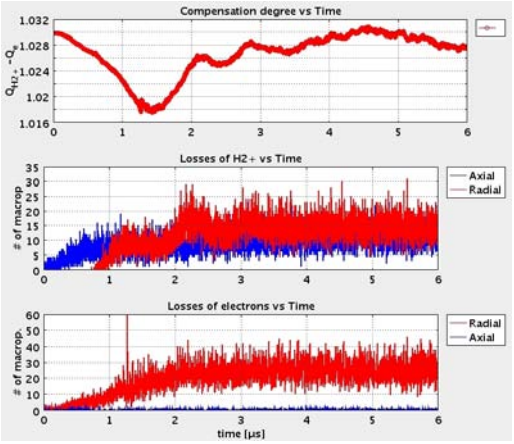

Figure 4: History of total compensation degree (upper panel), and of radial-axial losses (in macroparticles per time step)

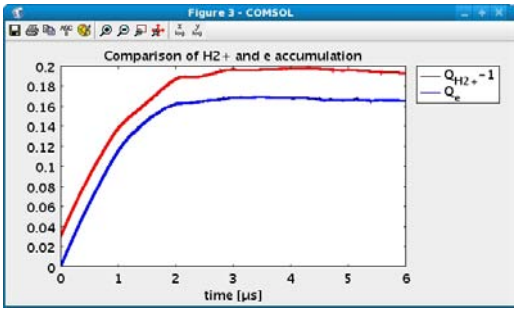

Figure 5: History of accumulated fractions of ions and electrons

3 Results

Result of PIC-MC simulation for the case $T_i = 1$ eV and $\phi_{PA} = 0$ are shown in Figs. 2-7. This simulation takes 36 h on a 7 core workstation.

An important result found by the 2D fluid model was that the distribution of H_2^+ ions (upper panel of Fig. 2) was more diffused than the beam profile: cloud of H_2^+ ions extends also outside the beam. The PIC-MC simulation result in the Fig. 2 confirm this fact, even if the logarithmic scale tends to make halo fluctuation more visible. In Fig. 2 note that $\phi_{PA} = +25$ V for the fluid model and $\phi_{PA} = 0$ V for PIC-MC, but this locally affects only the PA region.

The diffusion of H^{2+} is more clearly visible in Fig. 3, referring to central section $z = \frac{1}{2} z_h$ and final time $t = 0.006$ ms; the difference between primary density n_{H-} and secondary density $n_2 - n_e$ is the reason of the double charge layer.

Code results include also the time history of some space integrated quantities; from the upper panel of Fig. 4 and from Fig. 5 we note that total compensation $Q_2 - Q_e$ reaches equilibrium rapidly, while Q_2 and Q_e seems to follow similar growth, at least for the particular initial condition chosen ($Q_2 = 1.03$ and $Q_e = 0$). Radial losses means count of the macroparticles exiting from the upper and lower boundaries; axial refers to macroparticles exiting from the $z = 0$ boundary; a continuous time averaging is applied to make trends more visible. Axial and radial losses of H_2^+ seems to be roughly equal, notwithstanding that lengths of the boundaries is so much different. In the electron case axial losses are negligible, since they are repelled by the field near PA hole.

A potential map (at final time) is shown in Fig. 6; the negative values near $z = 0$ are due to loss of H_2^+ ions near the PA, which weakens the SCC, so that the negative primary beam charge locally overwhelms the SCC. The double layers of the net space charge en_0n_a on both beam edges is evident also in the lower panel of Fig. 6, and is similar to charge layers found by the fluid model, as shown (for a different n_b profile) in Fig. 5 of Ref. [5].

Figs. 6 and 7 also confirm the complicate field pattern near the PA grid.

Simulations for $\phi_{PA} = +25$ V and other values, and/or more macroparticles, are well in progress. Using different typical beam profiles, the dependence of the cloud radius from the ion temperature is also to be investigated.

4 Discussion: Monte Carlo vs fluid model

The original reason to develop a PIC-MC (Particle In Cell-Monte Carlo) code was that, even if computationally much more intensive than fluid models, PIC-MC simulations are the standard choice[2, 12] because they are simpler to define and they naturally follow the time evolution of the system; in particular they verify whether SCC stationary equilibrium is stable or not. We anyway see that granularity noise (roughly proportional to $N_2^{-1/2}$) has visible consequences (especially evident in Fig. 7) and this fact

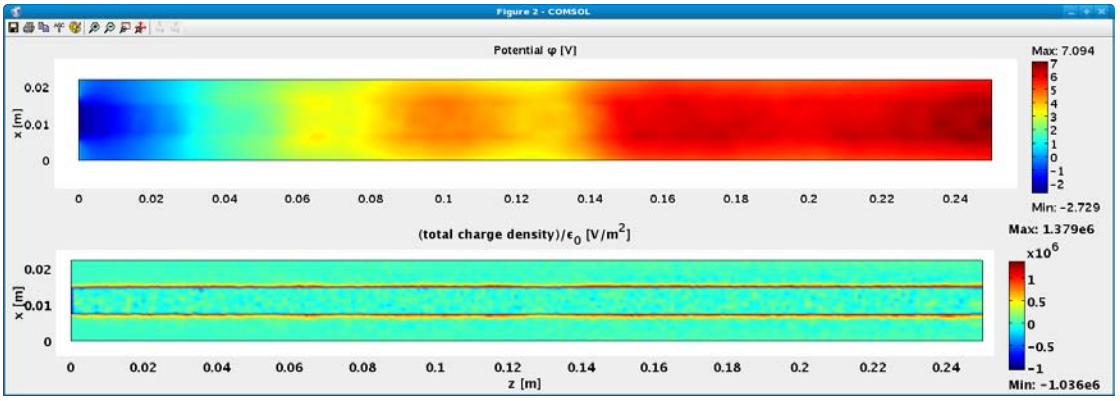

Figure 6: Upper panel is a surface plot of ϕ; lower panel shows the total charge density, typically near zero but with double charge layers aside the beam

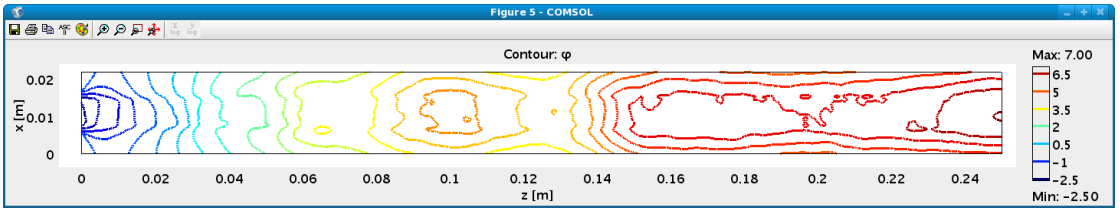

Figure 7: Contour plot of ϕ

seems to require stronger smoothing schemes. Moreover, in Fig. 3 our main smoothing scheme (applied to total space charge) is shown: note that more smoothing will substantially deform the body of the space charge, while less smoothing will make granularity fluctuation more evident.

It should be noted that results of fluid model and PIC-MC are similar, with differences mainly due to implementation details (beam shape trapezoidal or parabolic, recessed or flat input plane); so that a fluid equilibrium (or an analytical guess of its solution) was used to start PIC-MC from a nearly compensated state.

Apart from fine tuning of smoothing techniques, future work should take in consideration joining of fluid and PIC-MC codes; for example, the nonlinear solver of a fluid model may start from the noisy (but probably stable) equilibrium found by a PIC-MC simulation.

References

[1] A. T. Holmes, *Beam Transport*, in *The Physics and Technology of Ion Sources*, (ed. I.G. Brown), J. Wiley, NY, 1989

[2] N. Chauvin et al., Proceedings of LINAC08, Victoria, BC, Canada, 242

[3] I. A. Soloshenko, Transportation of intensive ion beams, Rev. Sci. Instrum. **69**, 1359 (1998)

[4] A. BenIsmail et al, Space charge compensation studies of hydrogen ion beams in a drift section Phys. Rev. ST-AB 10, 070101 (2007)

[5] M. Cavenago, P. Veltri, Space charge compensation of negative ion beams, in Comsol 2010 User Conference, CD-ROM (2010)

[6] T. Inoue et al., "Design of neutral beam system for ITER-FEAT", Fus. Eng. and Design 56-57 (2001) 517-521

[7] H. P. L. de Esch, R. S. Hemsworth, and P. Massmann, SINGAP: The European concept for negative ion acceleration in the ITER neutral injectors, Rev. Sci. Instrum., **73**, pp1045-1047 (2002)

[8] P. Agostinetti et al., "Design of a low voltage, high current extraction system for the ITER Ion Source" , in *Negative*

Ions Beams and Sources, 1st Int. Symposium, AIP CP **1097**, (ed. E. Surrey, A. Simonin, AIP, Melville, 2009), p. 325

[9] P. Veltri, P. Agostinetti, G. Serianni, V. Antoni M. Cavenago, Exploration of Operational Scenarios of the SPIDER Accelerator, subm IEEE-TPS.

[10] `http://www-amdis.iaea.org/ALADDIN` and links

[11] R. K. Janev, D. Reiter, and U. Samm, Collision processes in low-temperature hydrogen plasmas, Tech. Rep. Jul-4105, Forschungszentrum Julich (2003)

[12] G. Fubiani, H. P. L. de Esch, A. Simonin, R. Hemsworth, Phys. Rev. ST-AB, **11**, 014202 (2008)

[13] M. Cavenago, P. Veltri, F. Sattin, G. Serianni, V. Antoni, *IEEE Trans. on Plasma Science*, **36**, pp 1581-1588 (2008)

[14] M. Cavenago, P. Veltri, N. Pilan, P. Antonini, Simulations of Negative Ion Beams and Sources, in Comsol 2008 User Conference, CD-ROM (2008)

[15] Comsol Multiphysics documentation, (2007)